

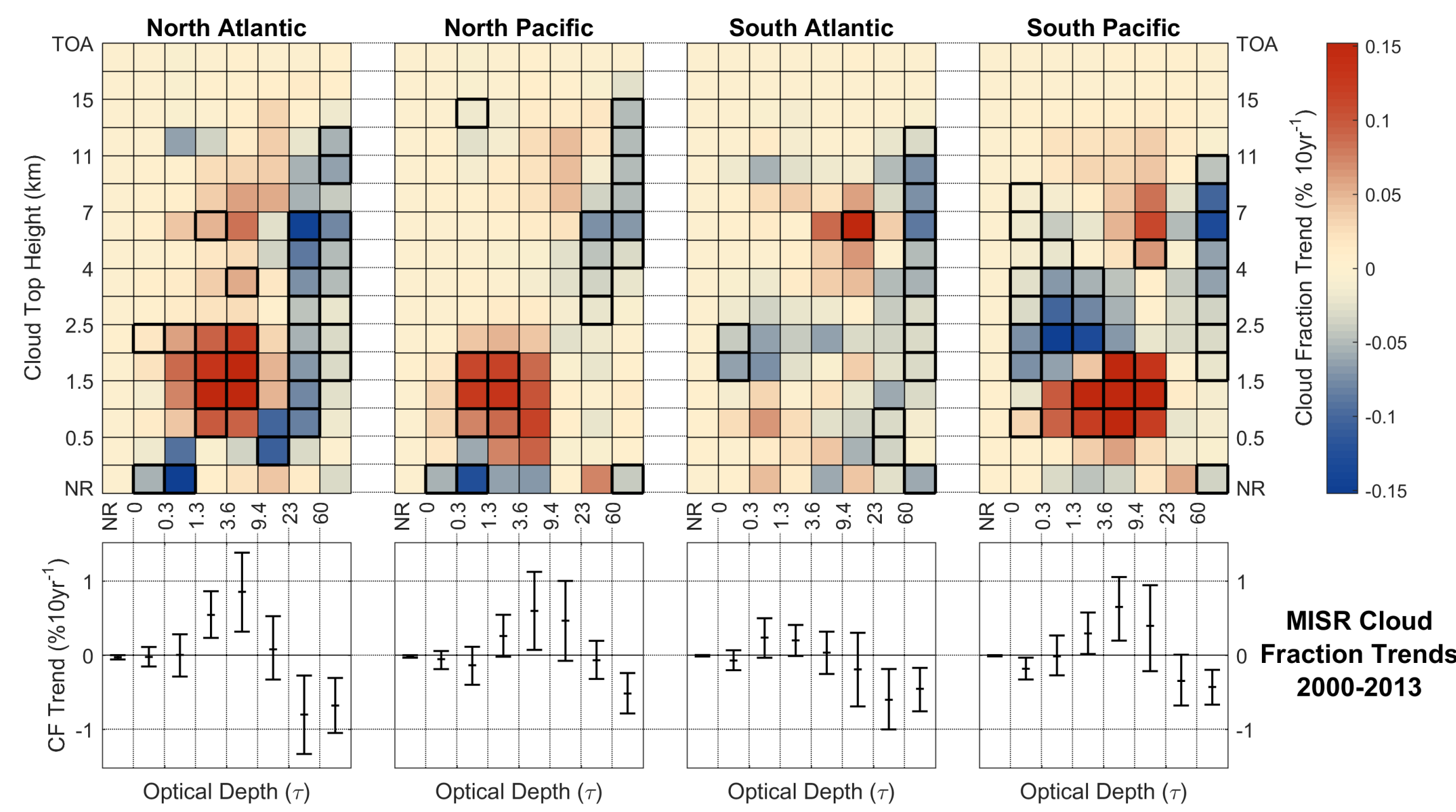
The response of cloud fraction to climate variability over the extratropical oceans as observed by MISR and MODIS



Andrew Geiss (avgeiss@gmail.com) and Roger Marchand (rojmarsh@u.washington.edu) -- University of Washington, Seattle, Washington

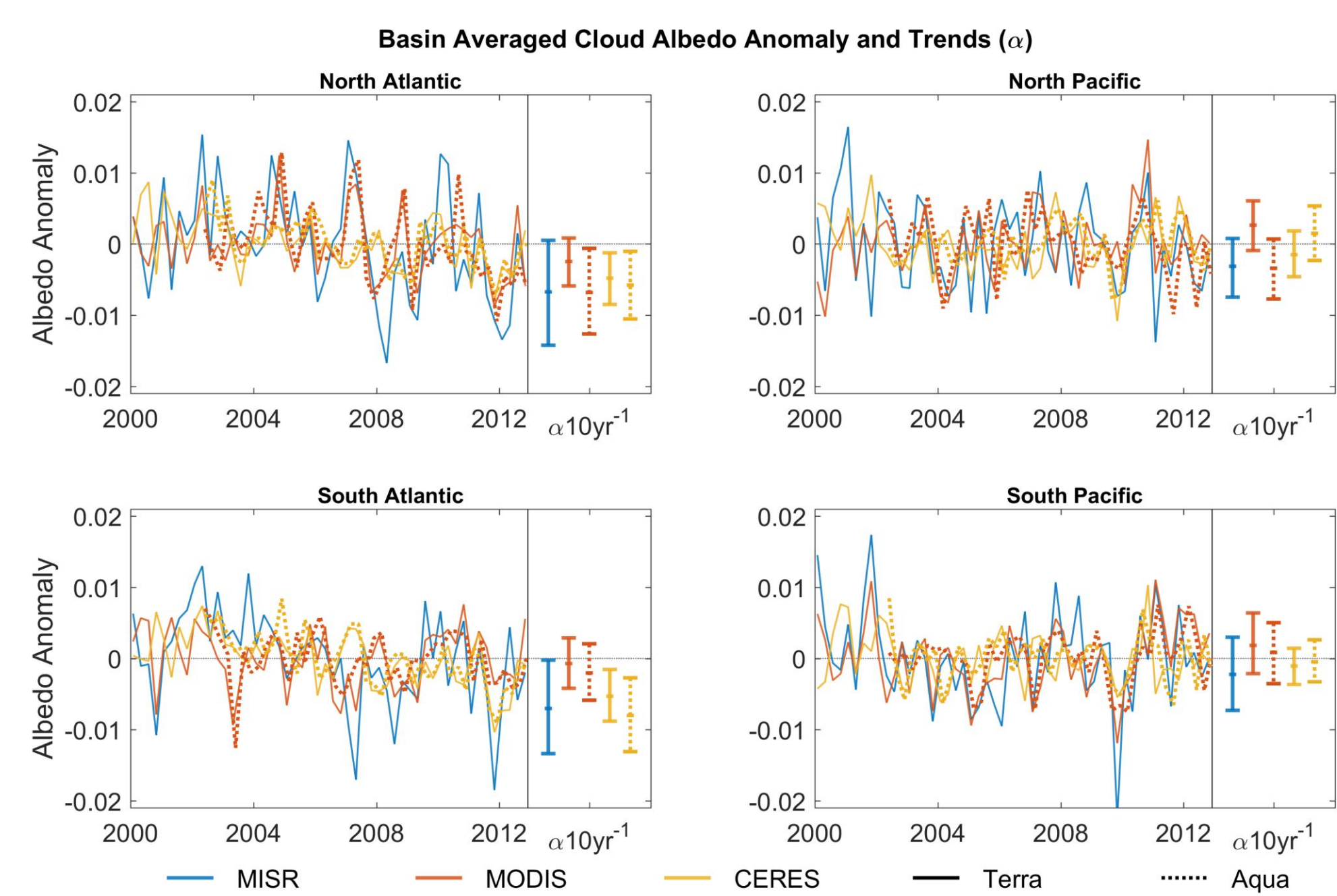
1. Background

The Multi-angle Imaging Spectro-Radiometer (MISR), and the MODerate resolution Imaging Spectro-radiometer (MODIS) both observed a reduction in optically thick cloud fraction over the extratropical oceans between 2000 and 2013 [1]. We examine these trends in the context of ERA-Interim reanalysis data, and assess their potential impact on cloud albedo and radiative forcing.



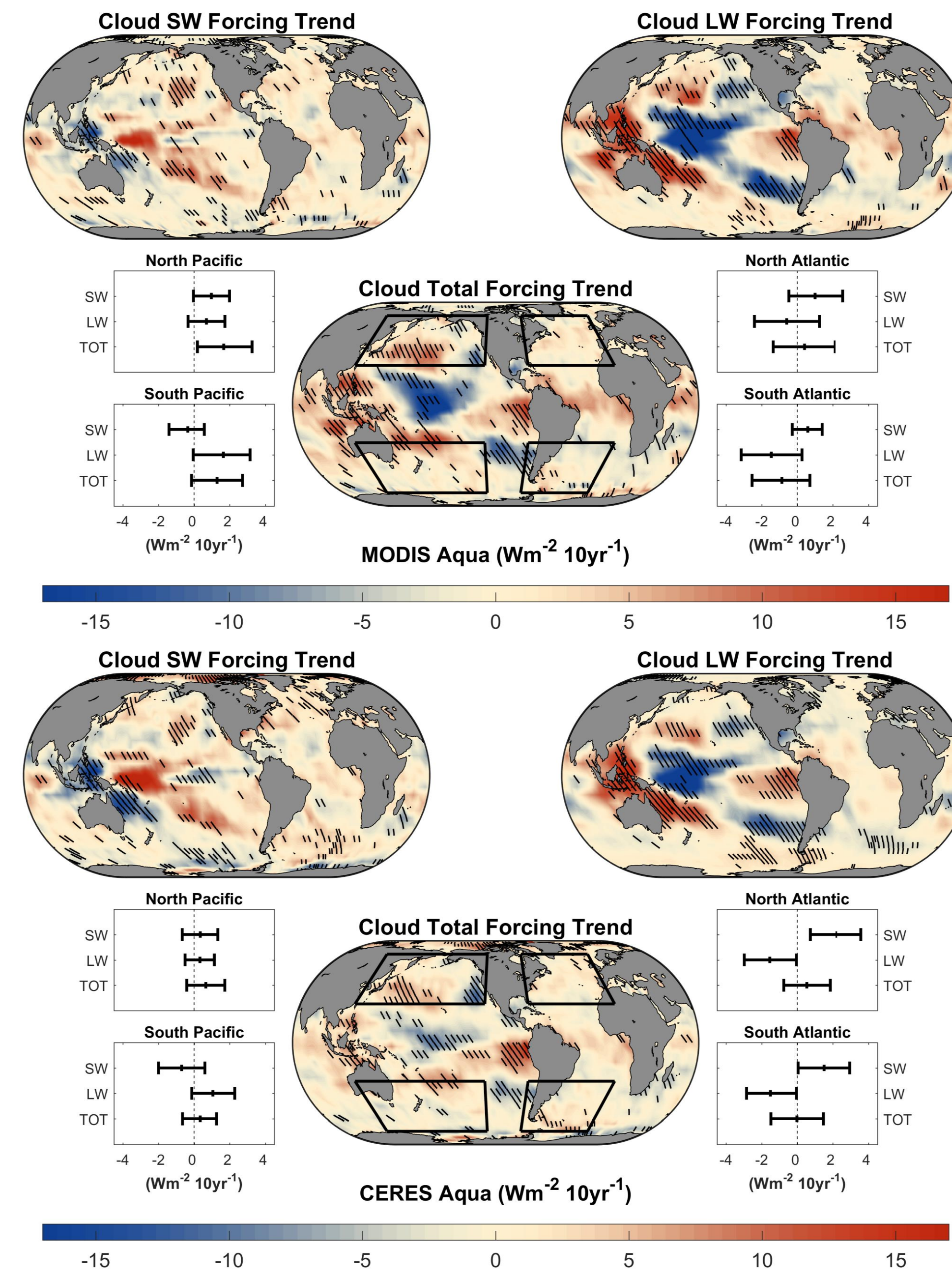
Above: linear temporal trends based on MISR cloud top height versus optical depth cloud fraction joint histograms, averaged spatially over four extratropical ocean basins. The trends are characterized by a reduction in optically thick cloud at most levels and an increase in low level cloud of moderate optical depth. Bold boxes and whiskers indicate 95% confidence.

2. Cloud Albedo



Time-series of spatially averaged cloud albedo anomaly in each of four ocean basins, and associated trends and 95% confidence intervals expressed as change in albedo anomaly per 10 years (right portion of each panel). MODIS (blue) and MISR (red) cloud albedos are estimated from cloud optical depth retrievals, and are compared to Clouds and the Earth's Radiant Energy System (CERES) (yellow) observed cloud albedos. Dashed lines represent instruments aboard EOS Aqua while solid lines are instruments aboard EOS Terra. Each of 5 instruments show a reduction in cloud albedo in the North and South Atlantic, while there is no consistent change in either Pacific basin.

3. Cloud Radiative Forcing

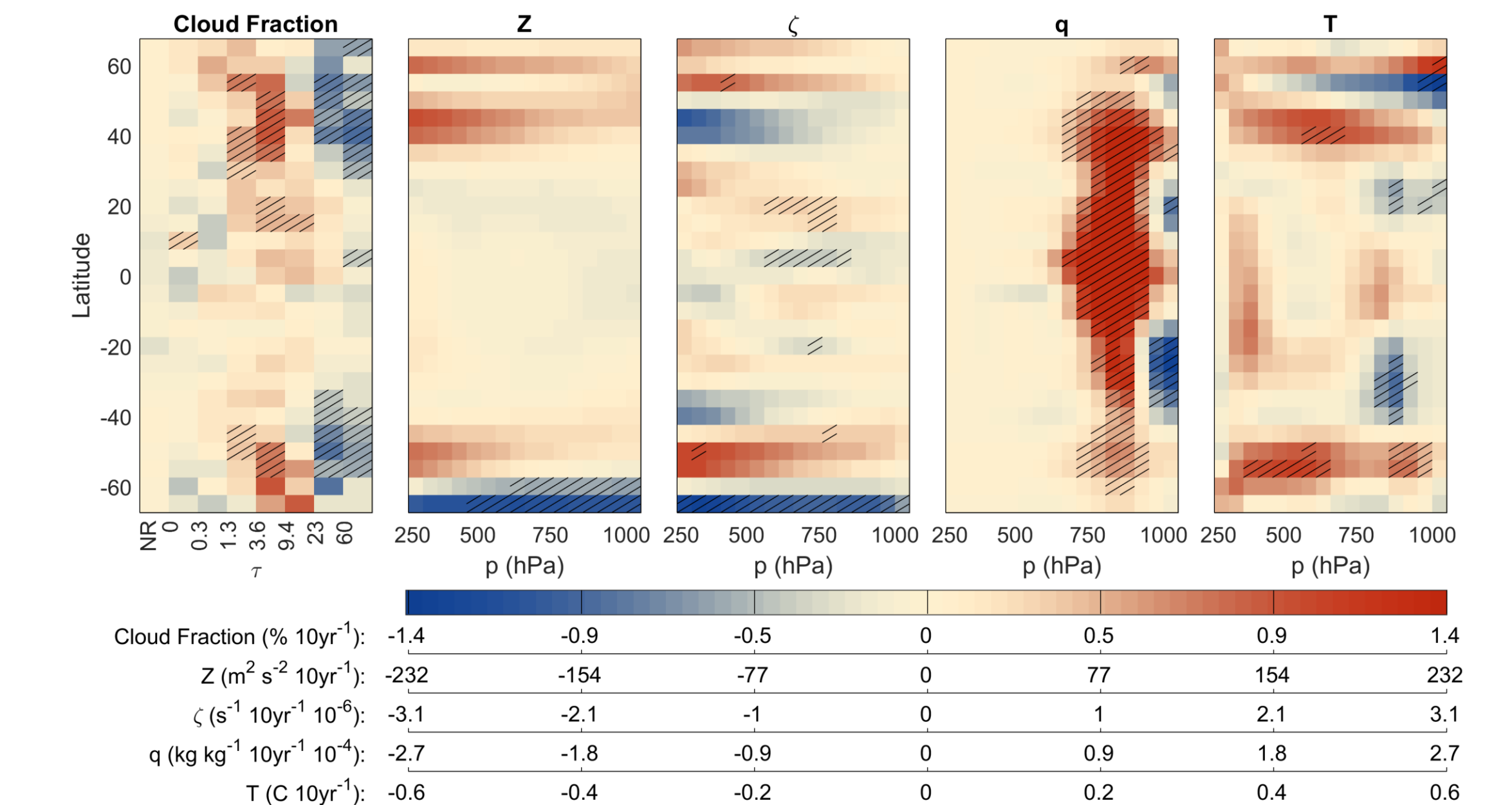


Estimated global distribution of cloud radiative forcing trends, using MODIS Aqua cloud fraction joint histograms and the MODIS cloud radiative kernels [2] (top). Cloud radiative forcing trends observed by CERES Aqua (bottom). Trends are broken down into longwave (upper right) and shortwave (upper left) components and the total (or net) forcing is shown at the bottom. Hatching denotes 95% confidence. Whisker plots show spatially averaged longwave, shortwave, and total cloud radiative forcing trends for each of the four extratropical study regions (boxed). Positive values indicate an increase in energy in the Earth system.

Based on estimated albedo trends (see 2), a positive trend in cloud radiative forcing is expected and is observed in both Atlantic regions. This is largely offset by negative cloud longwave forcing trends. No region shows a significant change in total cloud radiative forcing.

5. Overview

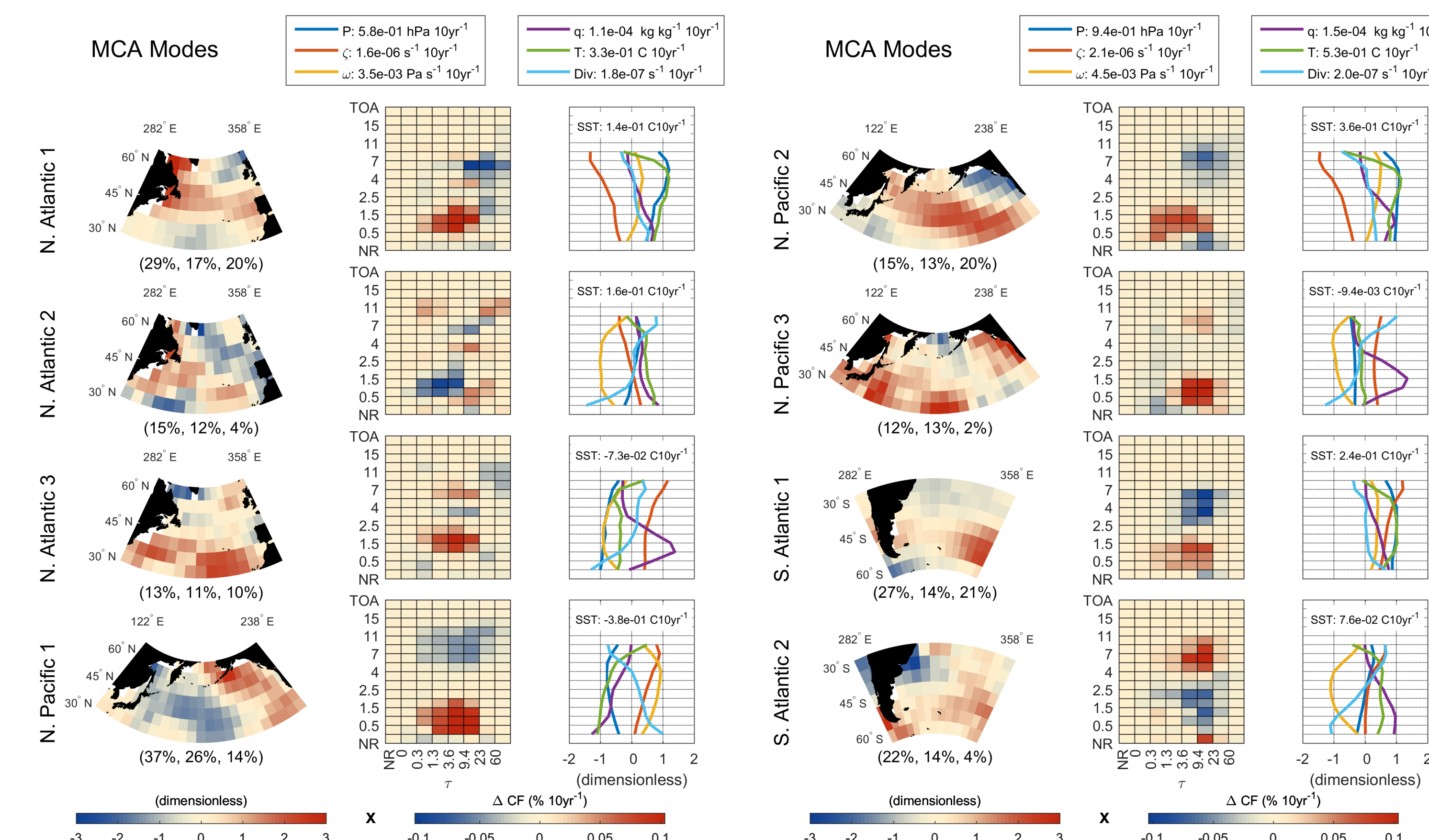
- MISR and MODIS have observed a reduction in optically thick cloud fraction over the extratropical oceans (2000 – 2013).
- This has resulted in a reduction in mean cloud albedo over the North and South Atlantic, with no significant change in the Pacific.
- There has been no significant change in cloud radiative forcing in the North or South Pacific or Atlantic observed by MODIS or CERES.
- The cloud fraction changes are associated with enhanced extratropical highs in these regions. In the Southern Ocean, this may be due to a trend in the Southern Annular mode.



Above: Trends in the zonal mean of MISR cloud fraction binned by optical depth, and 4 ERA-Interim reanalysis variables, (only over ocean). Hatching denotes 95% confidence. The latitudes where cloud optical depth has decreased also show enhanced geopotential heights, anticyclonicity, low level humidity, and temperature.

4. Relation to Synoptic Variability

Below: patterns in ERA-Interim variable profile trends and MISR cloud fraction joint histogram trends (2000-2013) identified by a Maximum Covariance Analysis (MCA). The MCA modes are computed by applying a singular value decomposition to the spatial covariance matrix between trends computed on the two datasets. Associated spatial loading patterns were obtained by projection of the ERA-Interim MCA modes (shown as vertical profiles) on to the original ERA trends. Listed with each mode is the fraction of the



covariance explained by that mode, followed by the fraction of variance explained in the ERA-Interim and MISR trends. Time series were derived for each mode by projection of the cloud fraction joint histogram patterns and associated spatial loading patterns on to the original MISR data. Below is a colored table of correlation coefficients relating each MCA mode time-series to several NOAA Climate Prediction Center (CPC) climate indices.

Time Correlation between CPC Indices and MCA Modes	NA1	NA2	NA3	NP1	NP2	NP3	SA1	SA2	SPT1	SPT2
Pacific Decadal Oscillation	-28	-27	-21	-56	-34	-39	-17	-19	-37	-26
North Pacific Index	19	16	25	54	53	36	3	20	18	11
Nino Region 4 Anomaly	-25	-25	-22	-24	-9	-20	-21	-22	-55	-31
Nino Region 3.4 Anomaly	-24	-30	-20	-26	-12	-18	-20	-24	-51	-28
Nino Region 3 Anomaly	-30	-13	-12	-22	-11	-10	-16	-23	-42	-23
Southern Annular Mode	18	17	2	19	17	7	21	27	25	34
East Atlantic/West Russia	-28	-32	-20	-15	-7	-12	-13	-19	-24	-15
East Pacific/North Pacific	-29	-22	-11	-12	-26	-4	-14	-15	-24	-15
Pacific/North American	-6	-4	-7	-36	-33	-27	10	-5	2	12
East Atlantic	-34	-22	-17	2	6	7	-2	-2	-23	-12
North Atlantic Oscillation	11	6	21	-10	-7	-11	-4	1	7	-5

The optical depth reduction is primarily seen in MCA modes: N. Atlantic 1, N. Pacific 2, S. Atlantic 1, and S. Pacific 2. Each of these are associated with increased pressure, geopotential height, and anticyclonicity; indicative of enhanced high pressure. In the Southern Ocean, this is correlated with the Southern Annular Mode.

Notably, N. Pacific 1 identifies cloud changes related to the Pacific Decadal Oscillation, while S. Pacific 1 identifies changes related to ENSO.

[1] Marchand, R., 2013: Trends in ISCCP, MISR, and MODIS Cloud-Top-Height and Optical-Depth Histograms. *J. Geophys. Res.*, **118**, 1941-1949, doi:10.1002/jgrd.50207

[2] Zhou, C., M. Zelinka, A. Dessler, and P. Yang, 2013: An Analysis of the Short-Term Cloud Feedback Using MODIS Data. *J. Climate*, **26**, 4803-4815, doi: 10.1175/JCLI-D-12-00547.1